Technical Memo

ECMWF
European Centre for Medium-Range Weather Forecasts

872

Quality control for GOES Geostationary Lightning Mapper Level-2 flash products

Philippe Lopez (Research Department)

October 2020

Series: ECMWF Technical Memoranda

A full list of ECMWF Publications can be found on our website under:
http://www.ecmwf.int/en/publications

Contact: library@ecmwf.int

Abstract

This technical document describes the homemade quality control procedure that was designed to remove spurious flashes found in the Level-2 flash product from the Global Lightning Mapper (GLM) on board NOAA's latest goestationary satellites GOES-16 and GOES-17. The algorithm is based on the identification of various types of spurious flash patterns using mainly geometrical criteria but also information about the spatial extent of each flash. An illustration of its good performance is given for various seasons of the year. Even though the number of erroneously detected flashes in the raw GLM Level-2 product has been decreasing in recent years thanks to NOAA's efforts, false flashes are still common today, making the application of the proposed quality control necessary prior to any usage for model validation or data assimilation purposes.

1 Introduction

NOAA's new-generation geostationary satellites GOES-16 and GOES-17 were launched on 19 November 2016 and 1 March 2018, respectively. In their current operational configuration, the sub-satellite point (SSP) is located at 75.2°W and 137.2°W, respectively. Both satellites are equipped with the novel Geostationary Lightning Mapper (GLM) which detects the optical signature of individual lightning pulses in the 777.4-nm oxygen band, where lightning emission peaks (Goodman *et al.*, 2013; Rudlosky *et al.*, 2019). GLM observations are continuously available over the entire field of view (FOV) of the instrument with a pixel resolution between 8 km at nadir and 14 km at the edge of the FOV. This document will lay the focus on GOES-16 GLM Level-2 (L2 hereafter) flash product, which provides information about flash location, time, horizontal extent (in terms of area) and radiant energy. An extension to GOES-17 is expected to be straightforward, due to its similarity with GOES-16.

The flash detection efficiency (DE) of the GLM instrument is usually higher during nighttime than during daytime, since the detection of individual lightning optical pulses is easier on a darker background. Typical values of flash DE vary between 75% (around local noon) and 88% (nighttime). However, an unexpected significant drop in flash DE (well below 50%) was identified towards the edge of the GLM's FOV, mainly over land (Koshak *et al.*, 2018). A tentative explanation involves the combination of (1) a reduction in the instrument's filter throughput at large boresight angles and (2) lower flash energies over land. In the case of GOES-16, this degradation mainly affects the western United States.

In contrast to the consequences of the limitations in sensor's DE, various other effects can cause the recording of false lightning flashes (Koshak *et al.*, 2018), which should be removed from the original data prior to any application, especially data assimilation. The present document describes the quality control (QC) procedure that has been developed at ECMWF to eliminate spurious flashes that remain in the GLM L2 product, despite the on-board and ground-segment filtering of the raw measurements. The main causes for spurious flash occurrences include contamination by sunglint, solar intrusions into the instrument, false identification of flickering bright cloud edges as lightning pulses due to instrument jitter, as well as thermal noise in the optical CCD. It should be noted that even though the removal of spurious flashes in the original GLM L2 product has been gradually improved by NOAA over time, the application of the QC procedure described here will still be required prior to any future assimilation of GLM in operations. It will also be instrumental in maximizing the period of availability of GLM data in future atmospheric reanalysis projects.

2 GOES GLM data

Practically, GOES-GLM L2 lightning flash data are read from original 20-second netCDF4 files named

`OR_GLM-L2-LCFA_G<SATNUM>_s<DATE_START>_e<DATE_END>_c<DATE_CREATION>.nc`

in which SATNUM denotes the satellite number (16 or 17) and all dates are formatted as YYYYDDDHHMNSSs (YYYY=year, DDD=day-of-year, HH=hour, MN=minutes, SS=seconds and s=tenths of second). These files are received in quasi-real time and are currently stored on ECMWF's File Storage system (ECFS) in the directory

`ec:/oparch/goes_<SATNUM>_glm_l2_lcfa/<YYYYMM>/<DD>/`

and in 15-mn (resp. 5-mn) tar files named

`OR_GLM-L2-LCFA_G<SATNUM>_s<DATE_START>_e<DATE_END>_c<DATE_CREATION>.tgz`

for dates before (resp. after) 0800 UTC 8 October 2019. Flash longitude, latitude, time, area and L2 product quality information is decoded from each individual netCDF4 file. Note that flash area is defined as the area of all GLM pixels affected by a given flash (in km^2). Figure 1 displays an example of all lightning flash locations observed by GOES-16 GLM over 24 hours on 15 August 2018 (after the application of the quality control described in this document).

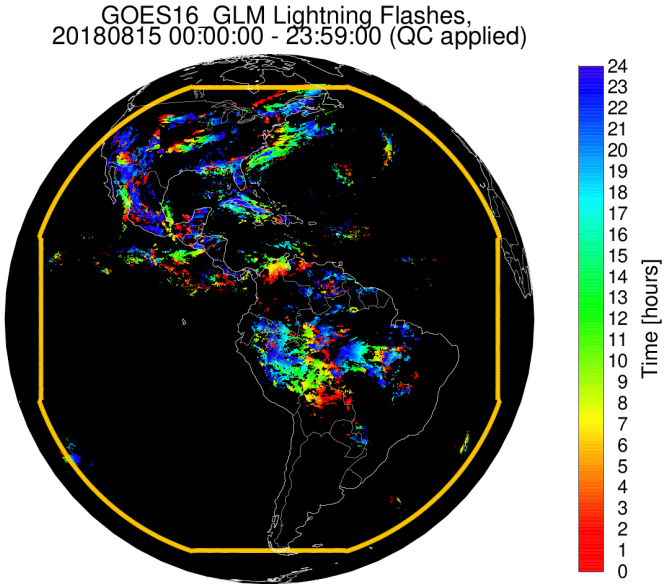

Figure 1: Example of 24-hour lightning flash observational coverage from GOES-16 GLM on 15 August 2018 (after QC). Colours indicate the UTC time of each flash. The thick orange contour shows the edge of the instrument's field of view.

3 Types of spurious flashes

Various types of spurious flashes can be identified in the original L2 flash products from GOES-16 GLM:

- Clusters of flashes associated with contamination by sunglint over the oceans or other water bodies.
- Loops of flashes due to direct illumination of the instrument's lens by sunlight during the eclipse season (near the equinoxes), which is likely to trigger blooming (i.e. sensor's pixel saturation).
- Isolated or adjacent horizontal lines of flashes caused by blooming induced by sunlight reflection inside the instrument.
- Regularly-spaced clusters of flashes also resulting from solar intrusion.
- Flashes that are isolated in both time and space and mainly due to thermal noise or platform jitter.

Figure 2 provides an illustration of those different types of spurious flashes as seen on the original L2 flash product on (a) 15 August 2018 and (b) 4 April 2019 over subdomains of the GOES GLM's field of view. In Fig.2.a, widespread contamination by sunglint can be identified at around 10°N in the east

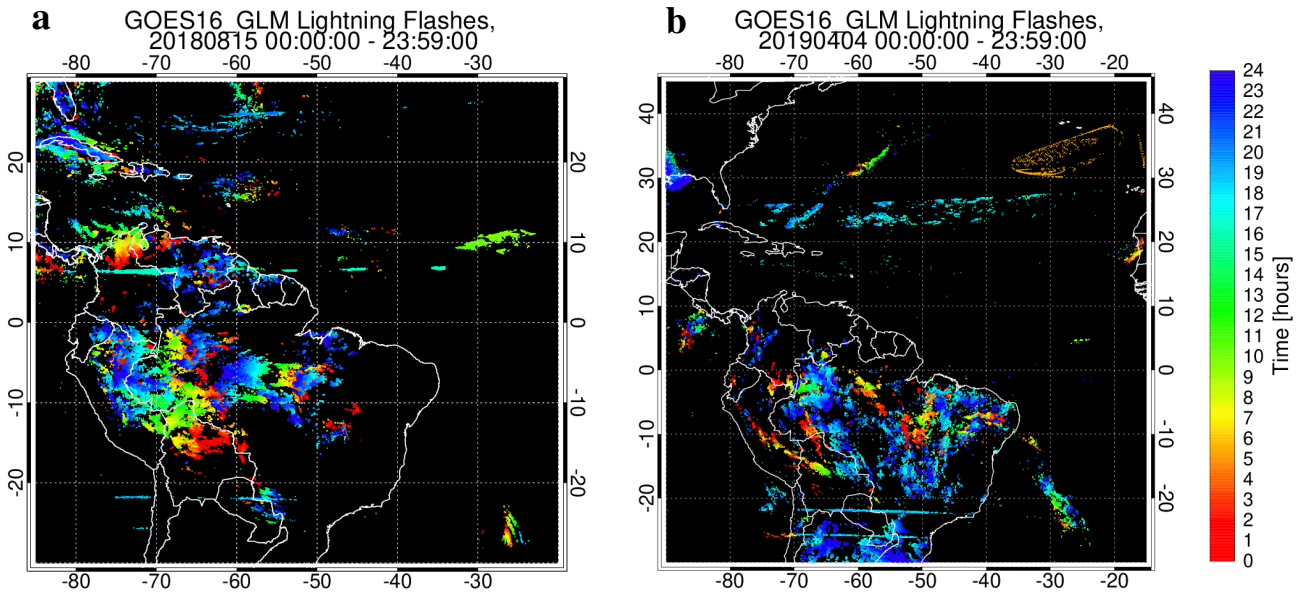

Figure 2: Original GOES-16 GLM L2 flash locations on (a) 15 August 2018 and (b) 4 April 2019, zoomed over South America and the Atlantic Ocean. Colours indicate the UTC time of each flash. Various types of spurious flash patterns can be easily identified (see text for details).

of the domain and at around 0900 UTC. Lines of spurious flashes appear all along the 7°N latitude at around 1700 UTC. Shorter lines also appear a little later along 22°S and 25°S as well as at about 26°N between 61°W and 54°W.

In Fig.2.b, odd-looking flash patterns due to straylight can be seen at around 0500 UTC in the northeast of the domain (orange dots), as expected during the eclipse season (near the equinox). In addition, between 1500 and 1800 UTC, spurious horizontal lines of flashes stretch across South America at around 22°S and 25°S, while horizontal bands of false flashes are obvious over the Atlantic between 22°N and 27°N.

It is worth stressing that the horizontal lines of false flashes appear to be slightly bent as a result of the cylindrical projection used in Fig.2. From the geostationary satellite point of view, these lines are truly straight.

4 Description of the quality control procedure

4.1 Removal of contamination by sunglint

Sunglint occurs when sunrays undergo specular reflection over the ocean surface or other water bodies such as lakes or even wide rivers. This phenomenon can be observed by day all year round and induces clusters of false flashes in GLM observations. For sunglint computations, time is subdivided into 15-mn timeslots. Figure 3 provides an illustration of the geometry involved in the calculations. The location of the centre of the region potentially affected by sunglint (orange shading) is computed for each time slot, using Gardashov and Eminov (2015). The radius R_{sg} of the sunglint region (in km) is assumed to be determined as

$$R_{sg} = R_{sg}^{max} - (R_{sg}^{max} - R_{sg}^{min})\cos(\alpha_{sg}) \tag{1}$$

where α_{sg} is the angle between the Earth's radius passing through the centre of the sunglint region and the line between Earth and the satellite (point S). Note that here R_{sg} is assumed to be measured along Earth's curved surface. Maximum and minimum sunglint radii R_{sg}^{max} and R_{sg}^{min} are set to 3000 and 500 km, respectively. Equation (1) implies that the sunglint region is assumed to become much wider away from SSP noon (for which $\alpha_{sg} = 0$). The algorithm rejects any flash that lies inside the sunglint region, that is if the centre angle γ between the flash's location (point F) and the centre of the sunglint region (point C) is lower than $\gamma_{max} = R_{sg}/R_{earth}$. In the latter formula, R_{earth} denotes the radius of the Earth.

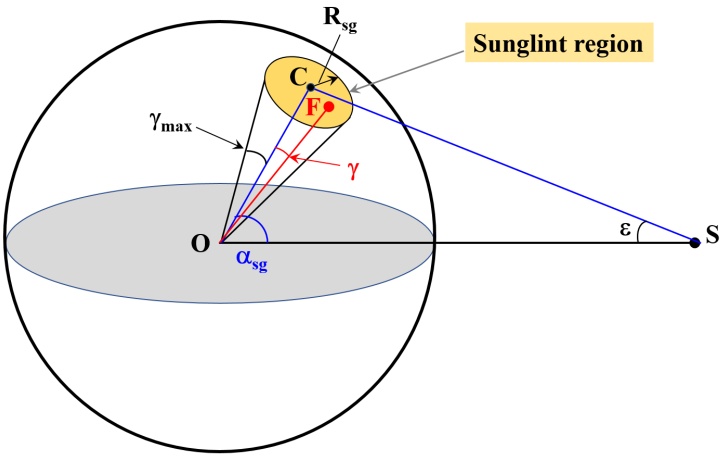

Figure 3: Sunglint geometry.

4.2 Removal of contamination by straylight

Straylight contamination only occurs during the eclipse season, which lasts for 44 days and is centred about each equinox (around March 20 and September 22). During this period, when the sun (as seen

by the satellite) is about to set or has just risen, straylight can directly illuminate the GLM telescope's lens. This often triggers blooming and the reporting of false flashes, which typically appear in the form of distorted loops of flashes near Earth's limb.

Therefore, the elimination of these spurious flashes from the L2 product is only applied:

- during eclipse season (namely from February 27 to April 13 and from August 30 to October 14).
- near sunrise and sunset times (i.e. within 1 hour before or after SSP midnight).
- if the viewing angle ε of the selected flash exceeds 6.5° (i.e. not too far from Earth's limb).

The viewing angle ε at a given point of latitude ϕ and longitude λ is given by

$$\varepsilon = \arctan\left[\frac{R_{earth}\sin\psi}{R_{earth}+z_{sat}-R_{earth}\cos\psi}\right] \tag{2}$$

where z_{sat} denotes the altitude of the geostationary satellite (typ. 35786 km), and

$$\psi = \arccos\left[\cos\phi(\cos\lambda\cos\lambda_{sat}+\sin\lambda\sin\lambda_{sat})\right] \tag{3}$$

in which λ_{sat} is the SSP longitude.

It should be noted that the revised filtering implemented by NOAA in mid-2019 has substantially, but not entirely reduced the occurrences of false flashes due to straylight in the original L2 product. Therefore the application of the above procedure remains necessary.

4.3 Removal of contamination by other solar intrusions

In addition to the previous straylight issue encountered around SSP midnight, two other types of spurious flash patterns are associated with solar intrusions around SPP noon (i.e. when the sun passes behind the satellite). These can be categorized as:
- Type 1: narrow lines of flashes persisting for up to 4 hours around SSP noon,
- Type 2: regularly-spaced clusters of flashes in the horizontal direction, mostly present within 30 minutes around SSP noon. For this type, the distance between neighbouring clusters is typically around 800 km and the width of each cluster is less than 100 km.

To filter out these spurious flashes, the geographical coordinates of each flash are converted to cartesian coordinates (X,Y) using the free PROJ4 software (https://proj.org/), as illustrated in Fig.4. The origin point of the cartesian grid coincides with the SSP. Cartesian coordinates vary between -5000 and +5000 km to encompass GLM's FOV and by definition the cartesian distance to the origin point is proportional to the viewing angle ε. The instrument's FOV is discretized into a $N_X \times N_Y$ grid of $\Delta X \times \Delta Y$-km boxes. N_X and N_Y are both set to 250, which implies that $\Delta X = \Delta Y = 40$ km. GLM's actual FOV is displayed in orange shading in Fig.4.

Time is discretized into 60-second timeslots. The window potentially affected by solar intrusions (referred to as the "intrusion window" hereafter) is assumed to span ± 4 hours around SSP noon, between times t_1 and t_2. The number of flashes inside each 40-km grid box and each time slot, denoted $h(i,j,t)$, is calculated, where indices i and j vary between 1 and 250.

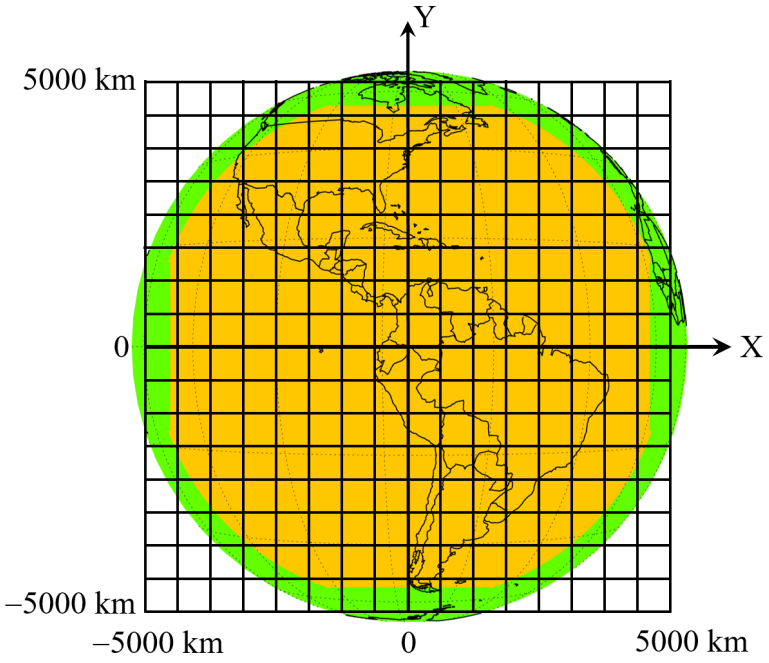

Figure 4: Schematic representation of the cartesian grid (X,Y) used to discretize GOES-16 GLM's field of view (shown with orange shading). Note that the grid spacing is not drawn to scale (the actual grid spacing is 40 km).

4.3.1 *Persistent narrow long lines of spurious flashes (Type 1)*

The histogram of flashes $h(i,j,t)$ is integrated both over the intrusion window and over the whole day

$$h_t^{intrus}(i,j) = \sum_{t=t_1}^{t_2} h(i,j,t) \tag{4}$$

$$h_t^{day}(i,j) = \sum_{t=1}^{N_t} h(i,j,t) \tag{5}$$

$$\tag{6}$$

The identification of narrow lines of spurious flashes relies on the convolution of the following quantity δ_1:

$$\delta_1(i,j,t) = \begin{cases} 1 & \text{if } h_t^{intrus}(i,j,t) \neq 0 \\ 0 & \text{otherwise} \end{cases} \tag{7}$$

with the following kernel K:

$$K = \begin{pmatrix} -2 & -2 & -2 & -2 & -2 \\ 0 & 0 & 0 & 0 & 0 \\ 1 & 1 & 1 & 1 & 1 \\ 0 & 0 & 0 & 0 & 0 \\ -2 & -2 & -2 & -2 & -2 \end{pmatrix} \tag{8}$$

This convolution is computed for each timeslot (index t) as

$$C(i,j,t) = \sum_{m=1}^{5}\sum_{n=1}^{5} K(m,n)\,\delta_1(i+m-3, j+n-3, t) \tag{9}$$

The convolution values are then summed in the horizontal direction to give

$$C_X(j,t) = \sum_{i=1}^{N_X} C(i,j,t) \tag{10}$$

which is used to define the following ratio:

$$R_C(j,t) = \frac{C_X(j,t)}{\max\left(\sum_{i=1}^{N_X}\delta_2(i,j,t), 1\right)} \tag{11}$$

in which

$$\delta_2(i,j,t) = \begin{cases} 1 & \text{if } C(i,j,t) > 0 \\ 0 & \text{otherwise} \end{cases} \tag{12}$$

Horizontal lines for which $|Y| < 3300$ km (i.e. approx. $\pm 32.5°$ of latitude) and $R_C(j,t) > 1.4$ and $C_X(j,t) > 35$ are flagged as suspicious. The horizontal spread S_X of a each suspicious line is then estimated as

$$S_X = \sum_{i=1}^{N_X} \delta_3(i,j,t) \tag{13}$$

where

$$\delta_3(i,j,t) = \begin{cases} 1 & \text{if } h_t^{day}(i,j) > 0 \\ 0 & \text{otherwise} \end{cases} \tag{14}$$

The final decision of rejecting all flashes inside a given suspicious line is taken if $S_X \geq 5$. Finally, to be conservative, all flashes in the two adjacent horizontal lines (indexed $j-1$ and $j+1$) are also rejected and the time window for the rejection is extended from time t_1 - 3600 and t_2 + 3600 seconds.

4.3.2 Regularly-spaced clusters of spurious flashes (Type 2)

The search for horizontally-aligned regularly-spaced clusters of flashes is limited to horizontal lines located within ± 240 km about the sunglint latitude and within the intrusion temporal window (i.e. ± 4 hours around SSP noon).

First, the number of flashes located inside a horizontal line and for a given timeslot is given by

$$h_X(j,t) = \sum_{i=1}^{N_X} h(i,j,t) \tag{15}$$

Then, the median value $M(j)$ of $h_X(j,t)$ is calculated over the intrusion window ($t_1 \leq t \leq t_2$) for each horizontal line (index j). Any horizontal line for which $h_X(j,t) > 2 * M(j)$ and $M(j) \neq 0$ is flagged as suspicious due to the high-temporal variability of its number of flashes. A comb-shaped mask is then

defined as illustrated in Fig.5. It is characterized by a set of 120-km wide "teeth" separated by a distance $D = 800$ km. For each time slot and each suspicious horizontal band, the number of hits $n(k)$ for a given X-position of the mask (index k) is defined as the total number of teeth overlapping at least one flash. The determination of $n(k)$ is repeated after successive horizontal shifts of the mask. In total, $\frac{D}{\Delta X}$ positions of the mask must be considered. The final rejection criterion is $\max_k[n(k)] \geq 4$, which is obtained for a position of the mask indexed as k_{max}. All flashes inside grid boxes that overlap with a tooth of the mask in its k_{max} position are rejected. To be conservative, the rejection is slightly extended in space and time. All

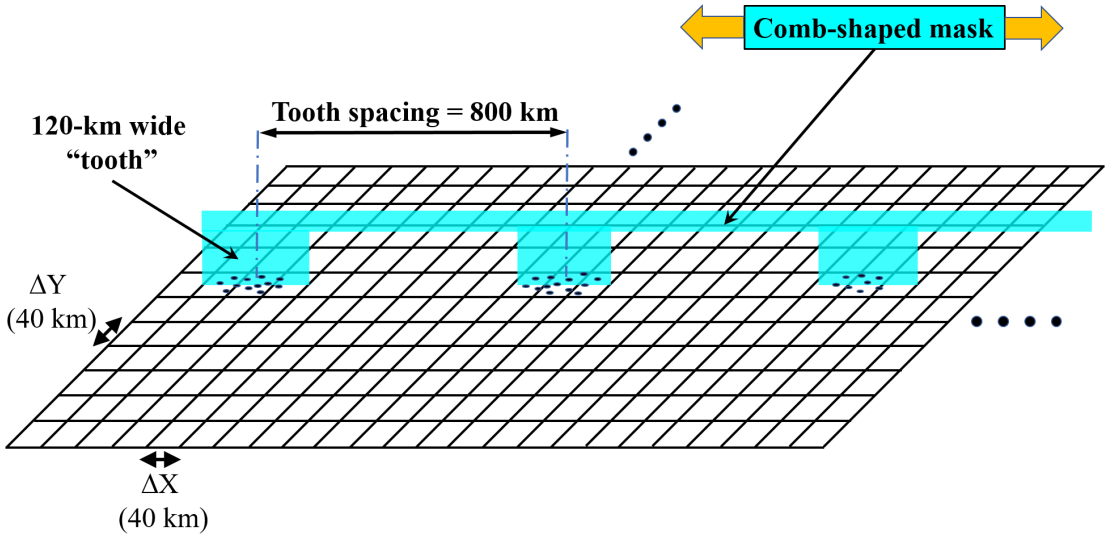

Figure 5: Illustration of the comb-shaped mask used for the identification of regularly-spaced clusters of spurious flashes due to solar intrusions into the instrument. For a given horizontal line, the maximum number of "hits" between the comb's teeth and individual grid boxes is computed over successive positions of the mask in the X-direction.

flashes located inside grid boxes that are immediately adjacent to contaminated boxes are also flagged as spurious. Furthermore, all flashes observed inside contaminated grid boxes within 4500 seconds before the first or after the last affected timeslot are also rejected.

4.4 Removal of remaining spurious small-area flashes

Even with the previous filtering applied, a few shorter lines of spurious flashes may remain, especially in the region of the Bahamas as well as off the Chilean coast. Further investigation showed that all flashes located in these spurious remaining clusters are characterized by a small area reported in the GOES GLM observations. Additional filtering is therefore applied in two independent steps:

1) All flashes located in a 40-km grid box (i, j) for which $|Y| < 3300$ km are rejected if

$$1 \leq h_t^{intrus}(i, j) < 20 \tag{16}$$

and if

$$\max_{k=1,n_f}(A_f[k]) < 150 \tag{17}$$

where n_f is the total number of flashes inside box (i, j) throughout the intrusion period and A_f denotes the total area of GLM pixels affected by a given flash (in km^2).

2) Remaining horizontal lines of contiguous boxes containing spurious flashes are identified from a cumulative index I defined for a given horizontal band. Index I is initially set to 0 and then incremented according to

$$I = I + 2^{p-1} \tag{18}$$

by looping over all boxes of the horizontal band for which

$$\text{median}_{k=1,n_f}(A_f[k]) < 150 \tag{19}$$

In Equation (18), p denotes the number of contiguous boxes that fulfill Equation (19). Counter p gets reset to 1 every time a new box fails to satisfy the latter criterion. This formulation ensures that a horizontal band containing many contiguous boxes that satisfy Equation (19) will have a large value of index I. The final criterion for rejecting all flashes inside the horizontal band is $I \geq 15$. The latter filtering is only applied to horizontal bands for which $2000 < |Y| < 3000$ km (i.e. for latitudes between approx. $\pm 18.6^\circ$ and $\pm 29.0^\circ$, in both hemispheres).

4.5 Removal of isolated flashes

The search for spurious isolated flashes is only applied to flashes that were not already flagged by the previous filtering. An isolated flag inside a given grid box is rejected if no other flash can be found within ± 1 hour and within $\pm \Delta X$ and $\pm \Delta Y$ (i.e. ± 40 km).

5 Performance assessment of the quality control procedure

The overall performance of the proposed quality control procedure is illustrated in Figs.6, 7, 8 and 9 which show maps of total flash counts per 0.2° grid box: (a) before QC, (b) retained after QC and (c) rejected by QC, for the periods 1 July - 31 August 2018, 1 December 2018 - 31 January 2019, 7 March - 7 May 2019 and 15 June - 15 August 2020, respectively.

Figure 6.a very clearly exhibits the various types of spurious flashes that are present in the raw GOES-16 GLM flash data. Clusters of false flashes due to contamination by sunglint are visible in the extreme northwest and northeast of the domain. Spurious lines of flashes extend eastwards from the Bahamas as well as across central South America, while odd-looking regularly-spaced patterns can be found in the tropical Atlantic, just to the north of the Equator. Figure 6.b-c shows that the QC procedure is successful at efficiently removing all those undesirable features. The total number of flashes given in the title of each panel indicates that overall 92.4% of original flashes are retained after QC.

In winter, Fig.7.a indicates that regularly-spaced clusters of flashes (in green) can be found off the Peruvian coast, while isolated lines of spurious flashes (in blue) affect the Pacific Ocean up to 2000 km west of the South American coast. Some contamination by sunglint is visible in the extreme southwest and southeast of the domain. Again, the QC algorithm is able to remove those unwanted flashes, as illustrated by Fig.7.b-c, while keeping 95.0% of original flashes that are deemed to be valid.

In Spring, Fig.8.a exhibits the typical signature of contamination by straylight, with individual loops of spurious flashes from consecutive days around the equinox overlapping all around the edges of Earth's disc. In addition, lines of false flashes can be very easily identified across the middle of the North Atlantic as well as across South America. The application of the filtering procedure (Fig.8.b-c) is able to efficiently clean the original L2 data, while preserving 79.4% of original flashes. Note that this lower

percentage of retained flashes compared to other seasons can be explained by the removal of numerous bad flashes caused by straylight.

Finally, Fig.9.a suggests that in 2020 the occurrences of bad flashes in the raw data have been substantially reduced by the additional QC recently implemented by NOAA, compared to the 2018 summer period shown in Fig.6.a. However, a few spurious lines of flashes can still be found at around 26°N over the Atlantic Ocean as well as just west to the north Chilean coast. Some contamination by sunglint is also present in the raw data off the western coasts of Spain and the United States. These features are successfully removed by the proposed QC procedure, as demonstrated in Fig.9.b-c, while 95.1% of raw flashes are retained in the quality-controlled dataset.

It must be stressed that an evaluation of the QC performance against independent observations from ground-based networks (GBNs) of lightning sensors would be very challenging and has therefore not be considered here. While GLM captures the optical signature of lightning, ground-based sensors usually detect electromagnetic signals (or sferics") emitted by lightning discharges at low or very-low frequencies, even from thousands of kilometres away. Because of their operating mode, GBNs at these frequencies are much better at detecting the usually more energetic cloud-to-ground (CG) flashes than cloud-to-cloud (CC) lightning flashes (Enno *et al.*, 2016; Said and Murphy, 2016; Poelman and Schulz, 2020). Typically, the DE of the current best GBNs is estimated to be around 90% for CG flashes but less than 50% for CC flashes. Furthermore, their DE can significantly vary in both space and time, with much lower values over open oceans than over land, due to the remoteness/lower density of land-based sensors. All this would make it very difficult to decide for instance whether a given flash which was reported by GLM but not by a GBN should actually be flagged as spurious. Besides DE limitations, flash location errors in both GLM and GBNs would make validation even more challenging. While flash location error should be well below 4 km at nadir for GLM as well as over land regions that are well-observed by GBNs, it is likely to reach 20 km or more when moving towards the edge of the GLM's FOV as well as over regions scarcely covered by GBNs, such as open oceans. Such errors would make matching individual flashes from GLM and GBNs rather tricky. Only lightning mapping arrays (LMAs) which operate at very-high frequencies can offer a DE close to 100% for both CG and CC flashes, together with flash location errors well below 1 km (Defer *et al.*, 2015). However, LMAs are limited to a few land sites and their horizontal range hardly exceeds 200 km. Therefore they would not allow a proper large-scale validation either, especially over the predominantly open-ocean regions observed by both GOES satellites.

Conclusions

A quality control algorithm has been designed to remove spurious flashes from GOES-16 GLM L2 flash product. The identification of unwanted flashes is primarily based on various geometric criteria and to a lesser extent on GLM's native information about flash area. It has been shown that the proposed QC procedure performs as expected throughout the year. Despite being rather conservative, the method does not eliminate too many valid flashes, since on average above 92% of original flashes are usually retained in the final product. This average ratio only drops down to 80% during the eclipse season (i.e. within $\pm$22 days of each equinox). Even though a reduction of spurious data occurrences in the raw GLM flash L2 product was achieved following NOAA's efforts to improve their upstream QC in 2019, false flashes are still common in recent data. These must be removed prior to any application of the GLM observations to validate the model and, even more crucially, in any attempt to assimilate lightning data in an NWP system. Indeed, assimilating the wrong information about convective activity could be really harmful to the quality of output weather analyses (and subsequent forecasts). The proposed QC procedure will

also be needed, should early GLM observations be assimilated as part of a future atmospheric reanalysis project. One can reasonably expect this filtering algorithm to work with GOES-17 GLM L2 flash data as well, even though a proper assessment of its performance will be required.

Acknowledgements

The National Oceanic and Atmospheric Administration (NOAA, USA) should be acknowledged for granting access to the GOES-16 GLM Level-2 product. Thanks also go to the European Organization for the Exploitation of Meteorological Satellites (EUMETSAT) for routinely sending GLM data to ECMWF via their EumetCast dissemination system.

References

Defer, E., Pinty, J.-P., Coquillat, S., Martin, J.-M., Prieur, S., Soula, S., Richard, E., Rison, W., Krehbiel, P., Thomas, R., Rodeheffer, D., Vergeiner, C., Malaterre, F., Pedeboy, S., Schulz, W., Farges, T., Gallin, L.-J., Ortéga, P., Ribaud, J.-F., Anderson, G., Betz, H.-D., Meneux, B., Kotroni, V., Lagouvardos, K., Roos, S., Ducrocq, V., Roussot, O., Labatut, L. and Molinié, G. (2015). An overview of the lightning and atmospheric electricity observations collected in southern France during the HYdrological cycle in Mediterranean EXperiment (HyMeX), Special Observation Period 1. *Atmos. Meas. Tech.*, **8**, 649–669, doi:10.5194/amt-8-649-2015.

Enno, S.-E., Anderson, G. and Sugier, J. (2016). ATDnet Detection Efficiency and Cloud Lightning Detection Characteristics from Comparison with the HyLMA during HyMeX SOP1. *J. Atmos. Oceanic Technol.*, **33**(9), 1899–1911, doi:10.1175/JTECH-D-15-0256.1.

Gardashov, R. H. and Eminov, M. S. (2015). Determination of sunglint location and its characteristics on observation from a METEOSAT 9 satellite. *International Journal of Remote Sensing*, **36**(10), 2584–2598, doi:10.1080/01431161.2015.1042119.

Goodman, S. J., Blakeslee, R. J., Koshak, J. W., Mach, D., Bailey, J., Buechler, D., Carey, L., Schultz, C., Bateman, M., McCaul Jr., E. and Stano, G. (2013). The GOES-R Geostationary Lightning Mapper (GLM). *Atmos. Res.*, **125-126**, 34–49, doi:10.1016/j.atmosres.2013.01.006.

Koshak, W., Mach, D., Bateman, M., Armstrong, P. and Virts, K. S. (2018). GOES-16 GLM Level 2 Data Full Validation Data Quality: Product Performance Guide For Data Users. 16 pages.

Poelman, D. and Schulz, W. (2020). Comparing lightning observations of the ground-based European lightning location system EUCLID and the space-based Lightning Imaging Sensor (LIS) on the International Space Station (ISS). *Atmos. Meas. Tech.*, **13**, 2965–2977, doi:10.5194/amt-13-2965-2020.

Rudlosky, S. D., Goodman, S. J., Virts, K. S. and Bruning, E. C. (2019). Initial Geostationary Lightning Mapper Observations. *Geophysical Research Letters*, **46**(2), 1097–1104, doi:10.1029/2018GL081052.

Said, R. and Murphy, M. (2016). GLD360 Upgrade: Performance Analysis and Applications. In *Proceedings of the 24th International Lightning Detection Conference & 6th International Lightning Meteorology Conference*, 18-21 April, San Diego, California, USA, 8 pages.

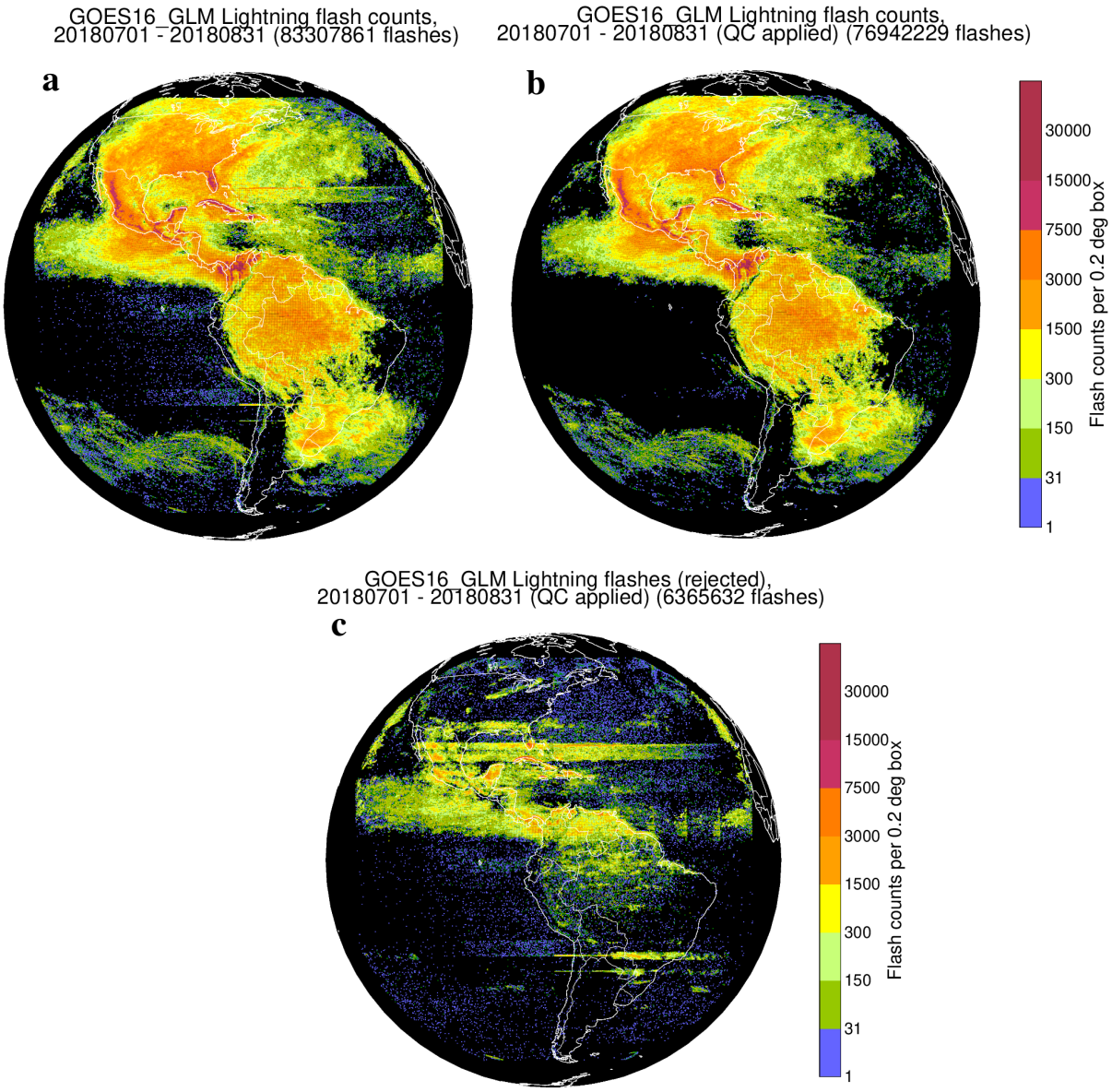

Figure 6: Total flash counts per 0.2° grid box (a) before QC, (b) retained after QC and (c) rejected by QC, from 1 July to 31 August 2018. It is worth remembering that the field of view of GOES-16 GLM (Fig.1) does not reach the edge of Earth's disk.

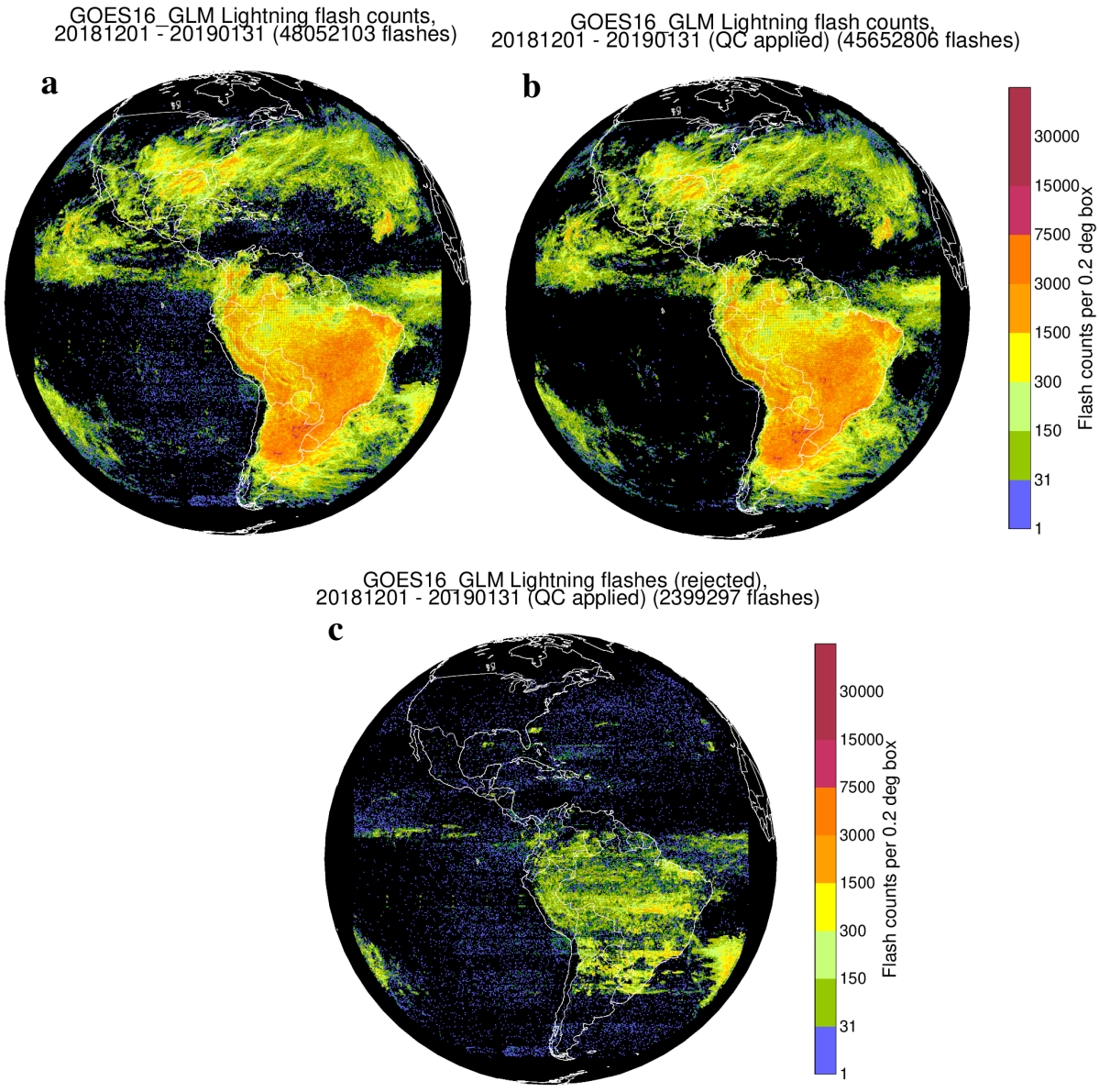

Figure 7: Same as in Fig.6, but from 1 December 2018 to 31 January 2019.

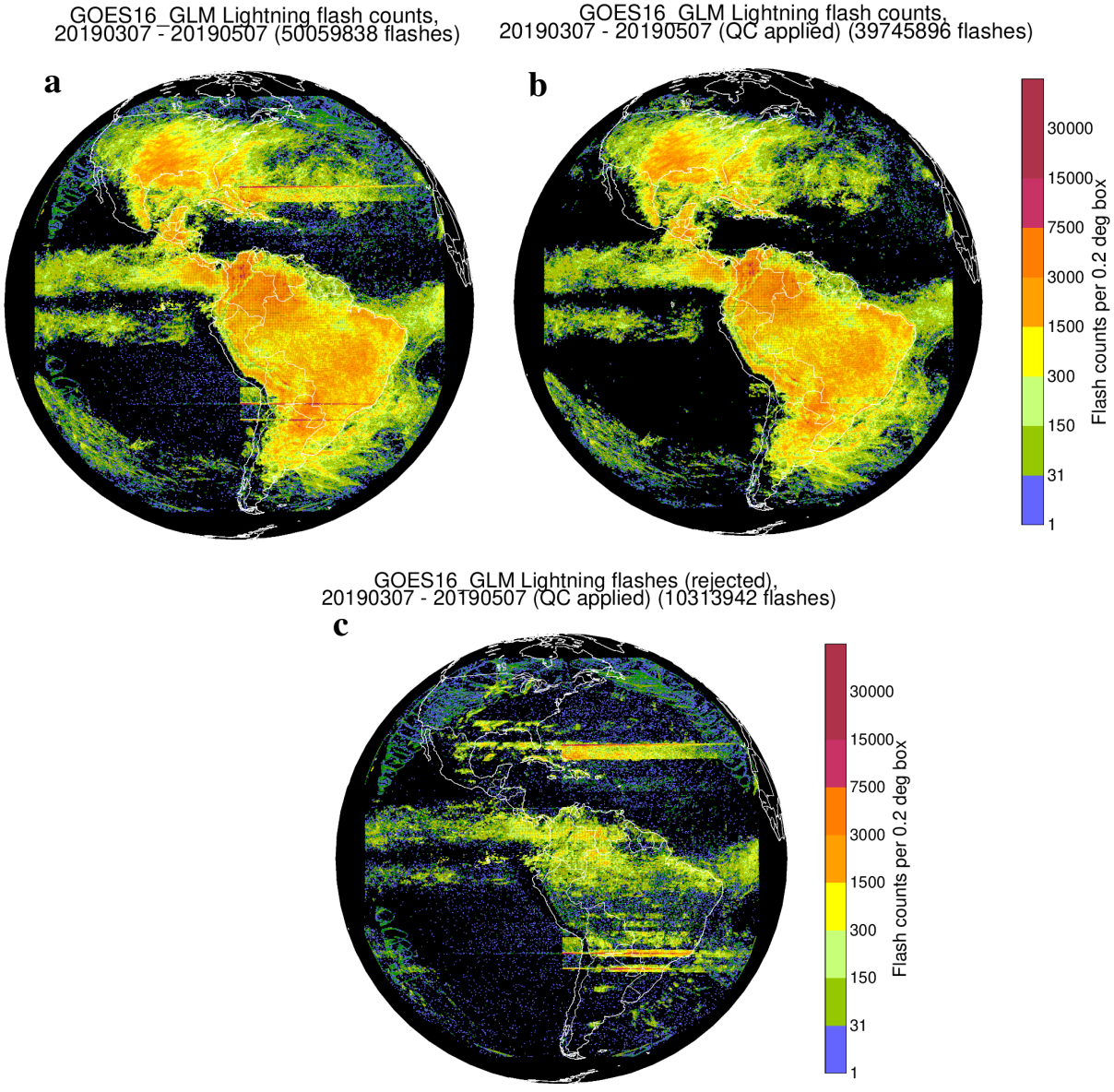

Figure 8: Same as in Fig.6, but from 7 March to 7 May 2019.

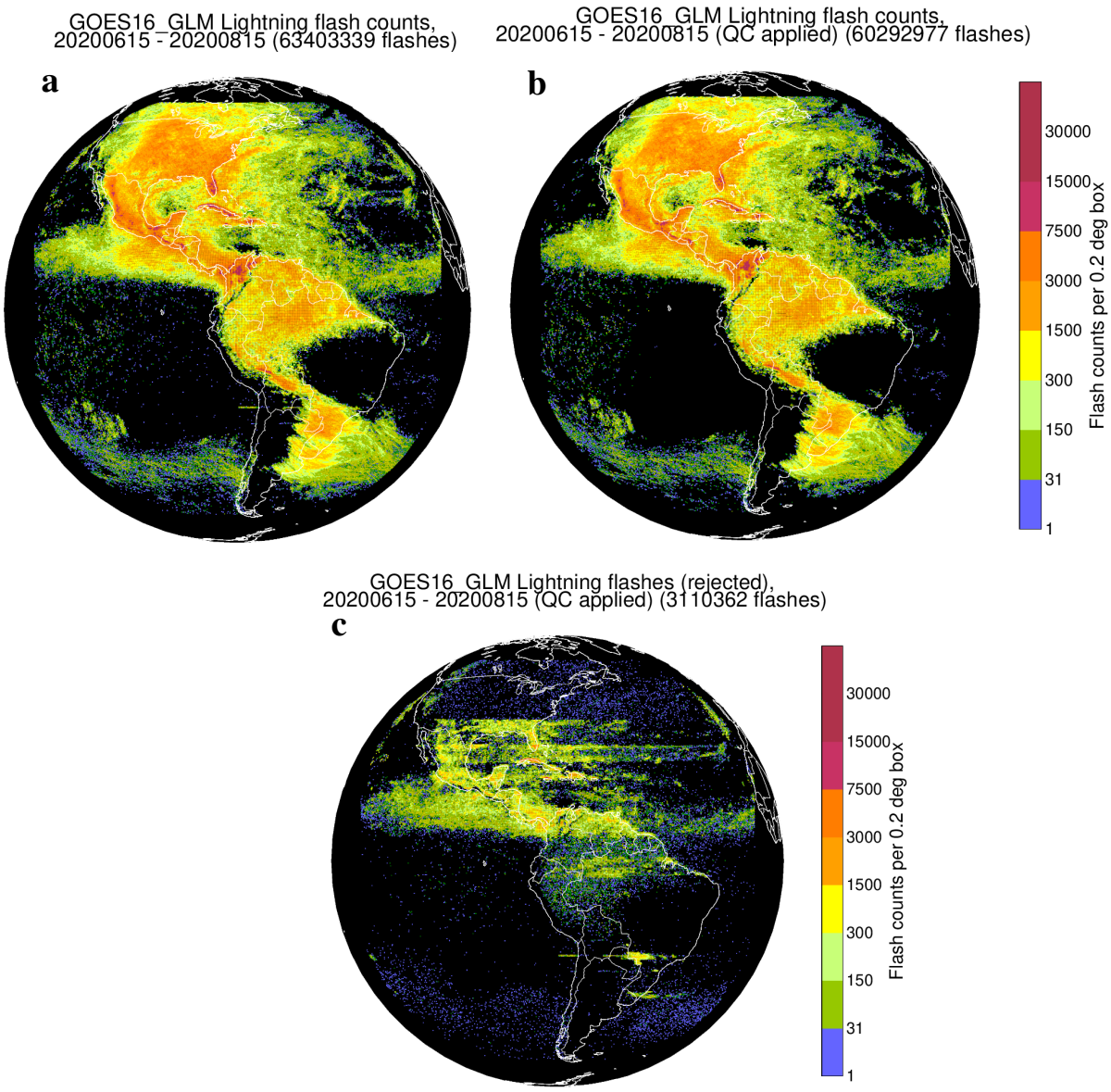

Figure 9: Same as in Fig.6, but from 15 June to 15 August 2020.